PCCP

Neighborhoods and Functionality in Metals

Journal:	*Physical Chemistry Chemical Physics*
Manuscript ID	CP-ART-10-2021-004787.R1
Article Type:	Paper
Date Submitted by the Author:	04-Mar-2022
Complete List of Authors:	Rajivmoorthy, Malavikha; Colorado School of Mines, Wilson, Tim; Colorado School of Mines, Chemistry Eberhart, Mark; Colorado School of Mines, Molecular Theory Group

Neighborhoods and Functionality in Metals

M. Rajivmoorthy[a], **T. R. Wilson**[a], **and M. E. Eberhart**[a,*]

[a]Molecular Theory Group, Colorado School of Mines, Golden, Colorado, USA; [*]To whom correspondence should be addressed. E-mail: meberhar@mines.edu

This manuscript was compiled on May 10, 2022

The fundamental construct of organic chemistry involves understanding molecular behavior through functional groups. Much of computational chemistry focuses on this very principle, but metallic materials are rarely analyzed using these techniques owing to the assumption that they are delocalized and do not possess inherent functionality. In this paper, we propose a methodology that recovers functional groups in metallic materials from an energy perspective. We characterize neighborhoods associated with functional groups in metals by observing the evolution of Bader energy of the central cluster as a function of cluster size. This approach can be used to conceptually decompose metallic structure into meaningful chemical neighborhoods allowing for localization of energy-dependent properties. The generalizability of this approach is assessed by determining neighborhoods for crystalline materials of different structure types, and significant structural defects such as grain boundaries and dislocations. In all cases, we observe that the neighborhood size may be universal—around 2-3 atomic diameters. In its practical sense, this approach opens the door to the application of chemical concepts, e.g., orbital methods, to investigate a broad range of metallurgical phenomena, one neighborhood at a time.

Keywords: nearsightedness | neighborhoods | dislocation | grain boundary | materials design | computational chemistry

1. Introduction

Chemical properties such as reactivity in molecular systems originate from functional groups, which retain their chemical identity regardless of the constitutive environment. Taking organic chemistry as the quintessential example, understanding the chemistry of a moderate number functional groups has made it possible to predict the properties of complex molecules. The functional group concept has also been useful in studying and manipulating the properties of many classes of materials, like carbon nanotubes [1], metal organic frameworks [2], and proteins [3]. Amongst those materials that have not benefited from this chemical analysis are metals—owing to the assumption that they are delocalized structures that do not possess an equivalent of functional groups. Here we test this assumption, by devising a methodology to determine and assess functionality associated with metallic materials.

Functionality is a well-studied chemical concept. An important early investigation by Bader and Beddall showed that it is possible to spatially partition molecules into volumes with well-defined energies and boundaries [4]. In his book, Bader mentions, "The primary purpose in postulating the existence of atoms in molecules is a consequence of the observation that atoms or groupings of atoms appear to exhibit characteristic sets of properties (static, reactive, and spectroscopic), which, in general, vary between relatively narrow limits". He defines this grouping of atoms as a functional group. He further adds, "In some series of molecules, the variation in the properties is so slight that a group additivity scheme for certain properties, including the energy, can be established"[5]. When such a condition exists, these atomic groupings are said to possess transferability - *i.e.*, their energy and other properties are insensitive to the local environment. In his earlier work to assess transferability of a bonded fragment, Bader observed that the difference in charge distribution and energy of CO in CO_2 and OCS is very small. He thus perceived a measure of transferability of functional groups being determined by the extent to which their charge distributions remain unchanged during transfer between systems [6–8]. These functional groups seemed to have an associated "neighborhood" wherein atoms felt its effect. Successive analyses that followed on the concept of transferability and its applications involved a rigorous investigation of charge distributions, and notably, not much attention was given to how the energy of functional groups evolve when moved from one constitutive environment to another [9–13].

A more recent perspective on functionality was presented by Prodan and Kohn as the theory of nearsightedness of electronic matter (NEM). NEM derives its name from the observation that atoms "see clearly" only nearby atoms [14, 15]. Rigorously, it posits that for a fixed chemical potential, the charge density, $\rho(\boldsymbol{r})$, and local properties originating from $\rho(\boldsymbol{r})$ are sensitive to changes to the external potential within some neighborhood with nearsightedness range R_c. Changes to the potential beyond R_c—no matter how large—do not significantly affect the density. NEM has been argued to be the foundation of many chemical concepts including "divide and conquer","chemical transferability", and Pauling's "chemical bond" [16–21].

To quantify NEM and transferability of functional groups, one must determine the neighborhood size wherein its effects are felt. In this context, of particular relevance is the work done in [10] to determine the "nearsightedness range". The authors investigated changes to ρ with changing molecular structure using the softness kernel. They argued that the effect of a functional group is felt only in a neighborhood about 3 atoms away, and structural changes that are farther from the neighborhood do not produce significant chemical effects. They showed that the correct view of nearsightedness and functionality is to picture it as a process under constant chemical potential consistent from the perspective that reactions are carried out in a solvent.

However, there is another equally valid way to envision functionality—more in keeping with Bader's idea of additivity—as the successive addition of environments around a functional group. In accordance with this view, we consider change in energy associated with adding successive coordination spheres about a central atom, and investigate the viability of these energy changes to determine neighborhood size, consequently serving as a means to describe metallic functionality. We propose a methodology to assess ρ sensitivity in these systems through changes in Bader atom energies. Identifying these neighborhoods in metals enables localization of structural perturbations that significantly alter energy.

When calculating Bader atom energies using the virial theorem there are several approaches (see SI for a more complete discussion). Of note is one method that treats the total kinetic energy as the sum of the noninteracting and correlation kinetic energy ($T_s + T_c$). Another often used approach represents the total kinetic energy by the product of the noninteracting kinetic energy and the virial factor (T_s*VF) [22]. Although both representations yield similar energy differences, those obtained through the T_s*VF representation, which implicitly include the exchange and correlation contributions to total energy, have been found to be more sensitive to the small contributions to the energy in unrelaxed systems, and to work well with metallic clusters. Accordingly, our calculations of Bader atom energies make use of this method.

As an initial step in validating our approach to identifying metallic functionalities, we explored the evolution of energy for a well-understood organic functional group, *i.e.*, an aldehyde, by growing the hydrocarbon chain to which it is attached. Our approach was intended to quantify the associated neighborhood of the aldehyde functional group. We considered $CHO(CH_2)_nH$ for our calculations, and varied n from 0 to 7. In accordance with the virial theorem, we utilized Bader partitioning to subsequently compute the energy of the aldehyde functional group (defined as the sum of the Bader energies of C, H and O) for each step, as summarized in Fig. 1 [5, 13].

Consistent with our expectations, the energy is an exponentially decaying function. The energy change beyond 3 carbon atoms from the functional group, is found to be less than three-tenths of an eV, coming to less than one-tenth of an eV between carbons 6 and 7. Our

The authors have no conflicts of interest to declare.

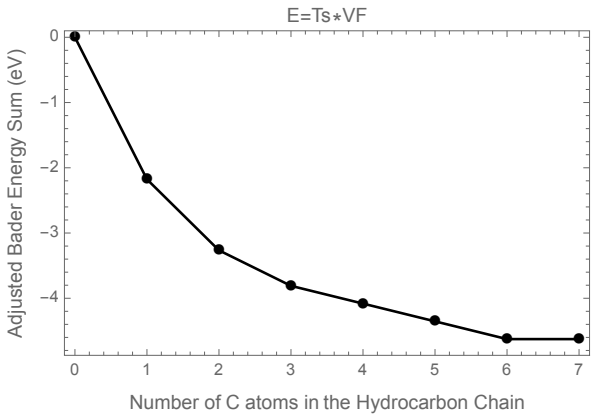

Fig. 1. The evolution of energy of an aldehyde group with increasing carbon atoms in the attached hydrocarbon chain.

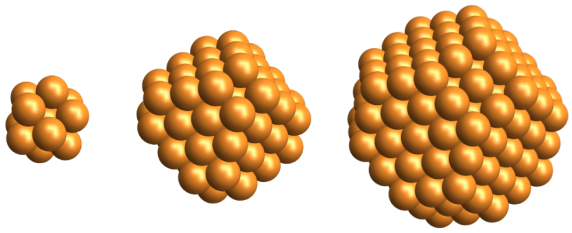

Fig. 2. A schematic of the series of cluster calculations for metallic materials is presented here. The cluster to the left indicates the central cluster Ω. The cluster in the middle indicates the central atom surrounded by 4 coordination spheres, and the one to the far right denotes a critical cluster with n coordination spheres.

observations from energy evolution retrieve similar results from the softness kernel analysis in [10]. Armed with these findings, we now move onto metals.

2. Neighborhoods in Metallic Materials

For the calculations summarized here, our general approach is to consider a "central cluster" Ω of radius R_Ω consisting of an atom and its first coordination shell—*i.e.*, first nearest neighbors. We isolate this cluster from its constitutive environment and compute its energy. Subsequently, we compute the changes to this energy $\Delta\varepsilon_\Omega$ as the atomic environment at successively greater distances from Ω are restored. Simply, we include concentric "spheres" containing second nearest neighbor atoms, third nearest neighbor atoms, and so on through n^{th} nearest neighbor atoms. A schematic of this series of cluster calculations is presented in Fig. 2. Beyond some R (or equivalently, n), we expect $\Delta\varepsilon_\Omega$ will asymptotically approach zero and be small in comparison to a phenomenon specific characteristic energies—in our case, cohesive energy. This "critical cluster," denoted as R_c, defines the neighborhood associated with the property of interest. We hypothesize that structural changes beyond R_c, no matter how large, will not significantly affect cohesive properties.

Through the aforementioned methodology we were able to calculate the central atom energy E_n^x as a function of adding successive coordination shells. Here x indicates the element and n indicates the number of coordination shells surrounding the central atom. Adopting this notation, the energy of an isolated atom is represented as E_0^x and the energy of single atom contained in an extended system as E_∞^x. It then follows that the formation energy, E_f, of an elemental crystal is given as $E_f = E_\infty^x - E_0^x$.

When crystalline systems are analyzed as progressively larger clusters, there exists a decreasing perturbative influence on the central atom due to the increasingly distant free surface.

This perturbation energy to the central atom as a function of n is given by $\Delta E_n^x = \Delta E_n^x - \Delta E_0^x$. As n increases, the value of ΔE_n^x will approach the crystal formation energy E_f^x. This perturbative effect can also be equivalently interpreted as stabilization of the central atom (or central cluster) as a result of embedding in progressively larger coordination environments. Both interpretations offer conceptual advantages when seeking to understand metallic functionality.

We now define a stabilization function, $\Delta\varepsilon_n^x \equiv \mid E_\infty^x - E_n^x \mid$, giving the magnitude by which the energy of an atom in an extended system is perturbed by the complete removal of all material beyond its n^{th} coordination shell. Where the system of interest is a perfect crystal, this function may be placed in a convenient form by adding and subtracting E_0^x,

$$\Delta\varepsilon_n^x = \mid (E_\infty^x - E_0^x) - (E_n^x - E_0^x) \mid = \mid E_f^x - \Delta E_n^x \mid \quad [1]$$

where $\Delta E_n^x \equiv E_n^x - E_0^x$ is a stabilization function giving the per atom energy change to Ω through the successive addition of n coordination spheres.

3. Computational Setup

Eleven crystalline elements (Al, Si, V, Cu, Nb, Mo, Tc, Ru, Rh, Pd, Ag) were modeled as clusters created with n varying from 0 to as large as 11. To model defect structures, we considered an Al dislocation, and grain boundaries in Cu and Fe which were also modeled as clusters. Density functional theory methods provided within the SCM chemistry and materials modeling suite [23, 24] were used. The per atom energy of Ω was found similarly using Bader partitioning precluding relativistic corrections. The omission of relativistic effects should not significantly effect our conclusions (see SI for more details).

ADF [1] cluster methods were used to calculate ΔE_n^x, while the BAND [2] package was used to calculate E_f [23–26] for the crystals. Eq. (1) was used to calculate $\Delta\varepsilon_n^x$ for a series of crystalline materials and defect structures, which we then use in a search for functionality.

4. Crystalline Neighborhoods

For the crystal systems, we constructed our calculations in sets of increasing complexity. In the first set we determined $\Delta\varepsilon_n^x$ of four crystals: diamond cubic (DC) silicon, a prototype covalent material; face centered cubic (FCC) aluminum, a free electron metal; FCC copper, a d-block metal with a full d-band; and body centered cubic (BCC) vanadium, a metal with a partially occupied d-band. These elements were chosen both because of their different crystal and electronic structures, and also because they could be modeled using the same basis set for both the BAND and ADF cluster calculations, thus minimizing inherent error in the calculated values of $\Delta\varepsilon_n^x$ (see SI). The focus of the second set of calculations was to develop an understanding of the factors causing variation to the stabilization function across elements sharing the same crystallographic structure. For this set of calculations we drew from the $4d$ transition metals: BCC niobium and molybdenum; hexagonal close packed (HCP) technetium and ruthenium; and FCC rhodium, palladium, and silver.

4.1. Silicon, Aluminum, Vanadium and Copper.

Silicon possesses the diamond cubic crystallographic structure. Its near neighbor shell structure is summarized in Table 1, with the central cluster Ω represented by a five atom cluster (Si_5) composed of a central atom and its four tetrahedrally coordinated nearest neighbors.

Relative to the energy of an isolated Si atom, E_0, the evolving per atom Bader energy of Si_5—as the coordination environment was increased to include a second, third, fourth and so

[1] amsterdam density functional
[2] accurate periodic DFT code

Table 1. The diamond cubic (DC) shell structure. Row 1: Number of the coordination shell. Coordination shell zero is the central atom. Row 2: Number of atoms in coordination shell n. Row 3: Total number of atoms in the cluster of n coordination shells. (Hard sphere representations of some of these clusters are provided in the SI.) Row 4: Radius of the cluster, $i.e.$ distance between the central atom and the atoms of the n^{th} shell in atomic diameters or equivalently nearest neighbor separations.

Coordination shell n	**0**	**1**	**2**	**3**	**4**	**5**	**6**	**7**	**8**	**9**	**10**	**11**
Number of n^{th} neighbors	0	4	12	12	6	12	24	16	12	24	12	8
Total atoms in cluster	1	5	17	29	35	47	71	87	99	123	135	143
Cluster radius	0	1	$2\sqrt{\frac{2}{3}}$	$\sqrt{\frac{11}{3}}$	$4\sqrt{\frac{1}{3}}$	$\sqrt{\frac{19}{3}}$	$2\sqrt{2}$	3	$4\sqrt{\frac{2}{3}}$	$\sqrt{\frac{35}{3}}$	$\sqrt{\frac{43}{3}}$	4

Table 2. Si atomic diameter, energy of formation, isolated atomic energy, and changes in central Bader atom energy resulting from the addition of cluster coordination spheres (ΔE_n^x) as described in the text. Distances are reported in Å and energies in eV. ΔE_{10} was not determined.

Si diameter (Å)	E_f	E_0	ΔE_1	ΔE_2	ΔE_3	ΔE_4	ΔE_5	ΔE_6	ΔE_7	ΔE_8	ΔE_9	ΔE_{11}
2.352	-5.42	-7865.72	-3.05	-9.01	-5.66	-5.55	-6.09	-6.71	-6.67	-6.12	-5.91	-5.79

on, up to eleven coordination shells—is reported in Table 2 along with the nearest neighbor distance of Si and its calculated formation energy, E_f.

These results are summarized graphically in the upper left of Fig. 3 where $\Delta\varepsilon^{\text{Si}}$ is depicted as a function of n. This figure represents the sensitivity of Ω to the retreating perturbation, that is, the distance over which the central cluster Ω can clearly see the free surface. When the energy goes to zero, from Ω's point of view, the surface has vanished. Plainly, when the free surface is infinitely distant from Ω, the per atom energy of Ω will be identical to that of an atom in crystalline Si. Hence beyond some point the decay of $\Delta\varepsilon$ will approach zero asymptotically. In fact, because for both ordered and disordered gapped materials[3] the change in the density due to a perturbation at R decays exponentially with R,[14] it is arguable that energy decay should not only be asymptotic but exponential.

Regardless, inspection of Fig. 3 reveals that the onset of the asymptotic/exponential decay begins with coordination shell seven, where the per atom energy difference between crystalline silicon and the central cluster Ω is on the order of an eV, decreasing to 0.36 eV at eleven coordination shells—thus defining the critical cluster size to be 3 atomic diameters beyond Ω.

Inherently, the variation of $\Delta\varepsilon$ originates from changes to the central cluster charge density [27]. And just as the energy of a central cluster within an infinitely distant free surface will be equivalent to that of a crystal, so too will its charge density be identical to the crystalline density. For all elemental crystals, equivalence between the central cluster and crystalline charge densities is required when the Bader atom surfaces of the central cluster are coincident with the crystalline Voronoi polyhedra (cells) about each atom. Quite generally, the difference between the surface of a cluster's Bader atoms and a crystal's Voronoi cells provides a measure of their charge density differences, which vanish when the two surfaces coincide [8].

A Bader atom's surface must contain local charge density minima. (In the chemical literature [5] these minima are called cage critical points to indicate that there is one such point interior to cages of bound atoms.) Plainly, an atom's local charge density minima may be a finite or an infinite distance from the atomic nucleus. If all the local minima are a finite distance from the nucleus, the surface of the Bader atom is topologically connected and the atom is said to be closed. On the other hand, if even one local minimum is located at infinity, the Bader atom surface is disconnected and the atom is said to be open. Importantly, for any open Bader atom there is a path lying entirely within the atom that runs from the location of the nucleus

[3] The systems modeled here are all gapped, in that the central cluster energy converges to within ~0.3 eV—our measure of significance—of the formation energy before the energy difference between the LUMO and HOMO is on the order of kT.

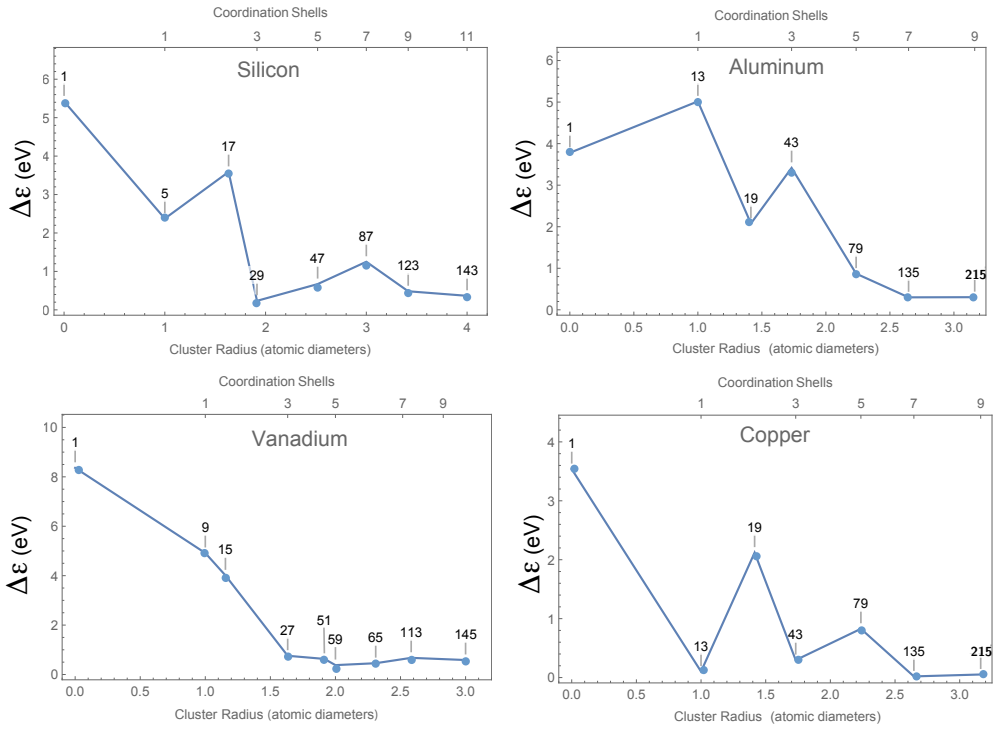

Fig. 3. The stabilization function ($\Delta\varepsilon_n^x$) for the elements Al, Si, V and Cu as a function of n. The callouts in the graphs give the number of atoms in the representative cluster. For example, an Al cluster representing a central atom and its first 7 coordination spheres will contain 135 atoms.

to a point at infinity. Quite simply, an open atom is characterized by a channel of decreasing charge density extending from the nucleus to the neighborhood of at least one infinitely distant point. In contrast, the surfaces of crystalline Voronoi polyhedra are necessarily connected. For example, the Voronoi cell of the diamond cubic structure is in a class of truncated tetrahedra.

As a means of clarifying this issue, consider the evolution of Ω's Bader atoms as more coordination shells are added [27]. In the case of Si, this process is represented in Fig. 4. The top-left frame depicts the Bader atom surfaces of Si_5, or equivalently the interatomic boundaries between the central atom and its first coordination sphere. This set of surfaces is constructed from four asymptotic—hence disconnected—surfaces. As a result, all the Bader atoms of the Si_5 cluster are open. In other words, around every point there is a direction in which the charge density is decreasing and thus local minima are infinitely distant from the central atom.

The boundary of the central Bader atom evolves with the addition of the twelve atom second coordination sphere to yield the Si_{17} cluster pictured in the top-right frame of Fig. 4. While the asymptotes separating the surfaces of this atom become steeper, the central Bader atom still extends to infinity. That is, running through all points near the central atom there is a path of decreasing charge density that leads to infinity. This path will pass through the "spikes" evident in the top-right frame of Fig. 4.

As depicted in the bottom-right frame of Fig. 4, it is with the addition of the fourth coordination sphere to make a Si_{35} cluster that the boundary of the central Bader atom is topologically connected and the atom is closed. It is at this point that the cages of bound atoms sharing the central atom as a common vertex are completed, which mandates a single local minimum at the center of each of these cages. In a sense, it is with the completion

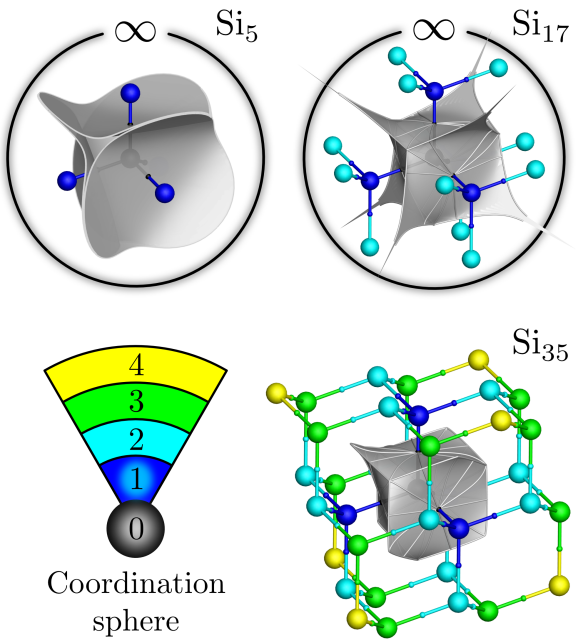

Fig. 4. Depiction of the central Bader atom surfaces in 5, 17, and 35 atom clusters (1, 2, and 4 coordination shells respectively). Nuclear positions are indicated by spheres colored according to coordination shell. In Si_5 (top-left) the central Bader atom remains clearly open in four regions, one of which is facing to the left of center, while elsewhere the Bader atom surfaces are essentially converged. With two coordination spheres (top-right; Si_{17}) those same open regions have closed coincident with topological cage points, and only slivers of very-nearly converged surfaces prevent the Bader atom from being closed. At four coordination spheres (bottom-right; Si_{35}) the Bader atom has closed completely. The open surfaces in Si_5 were truncated according to the $0.001e^-$ charge density isosurface.

of these cages, and the resultant closing of its Bader atom, that the central atom becomes isolated from the surroundings through an intervening shell of charge density.

While the central atom is closed with the fourth coordination shell, Ω closes at the seventh coordination shell, *i.e.* Si_{87}. It is here that the cages having a first coordination sphere atom as a vertex are completed. In fact, at this point the Bader atoms of Ω possess the topology of the Voronoi polyhedra of crystalline silicon. And, though Fig. 3 shows only a few points beyond the seventh coordination shell, $\Delta\varepsilon$ decreases monotonically (arguably exponential decay) through these points. Closing of the Bader atoms of the Ω provides a means to identify and characterize these crystalline neighborhoods.

Returning to the remaining crystals of the first set: Al, V, and Cu. The central cluster of the FCC metals (Al and Cu) is a cuboctahderon consisting of a central atom and its twelve nearest neighbors. The central cluster of BCC V is a nine atom cube with an atom at the cube center and its eight nearest neighbors located at the cube vertices. Pictures of these clusters along with analogues of Table 1 giving more information regarding the shell structure of FCC and BCC crystals along with the element specific cluster energy analogues of Table 2 are provided in the SI.

This information is also summarized graphically in Fig. 3 where $\Delta\varepsilon_n$ for the central cluster of each element is plotted as a function of n. In all cases, within ten coordination spheres $\Delta\varepsilon$ converges to within a fraction of an eV of the computed crystalline formation energy ($\Delta\varepsilon_9^{\mathrm{Al}}$, $\Delta\varepsilon_{10}^{\mathrm{V}}$, $\Delta\varepsilon_9^{\mathrm{Cu}} = 0.30$, 0.58, 0.05 eV respectively). More noteworthy however, though the onset of exponential decay is element dependent—two, three, and five coordination spheres for V, Al, and Cu respectively—beyond the point where the Bader atoms of Ω close (BCC clusters of five coordinations spheres and 59 atoms, and FCC clusters also of five coordination spheres and 79 atoms) $\Delta\varepsilon$ is monotonically decreasing or level.

4.2. 4*d* Metals.

The 4*d* transition metals required larger basis sets for the accurate determination of Bader atom energies. Because these basis sets were not available to the BAND calculations, a "basis set mismatch" error was introduced into the determination of $\Delta\varepsilon$. Specifically, we estimate that the formation energy calculated using the smaller basis sets available to BAND may be as much as 0.6 eV less than its estimated value from cluster calculations using larger basis sets (see SI). Nonetheless, for this set of calculations we are more interested in the stabilization function. Accordingly, ΔE as a function of the number of coordination shells for the BCC metals Nb and Mo; the FCC metals Rh, Pd and Ag; and the HCP metals Tc and Rh are shown in Fig. 5. The information contained in these figures is provided in tabular form in the SI.

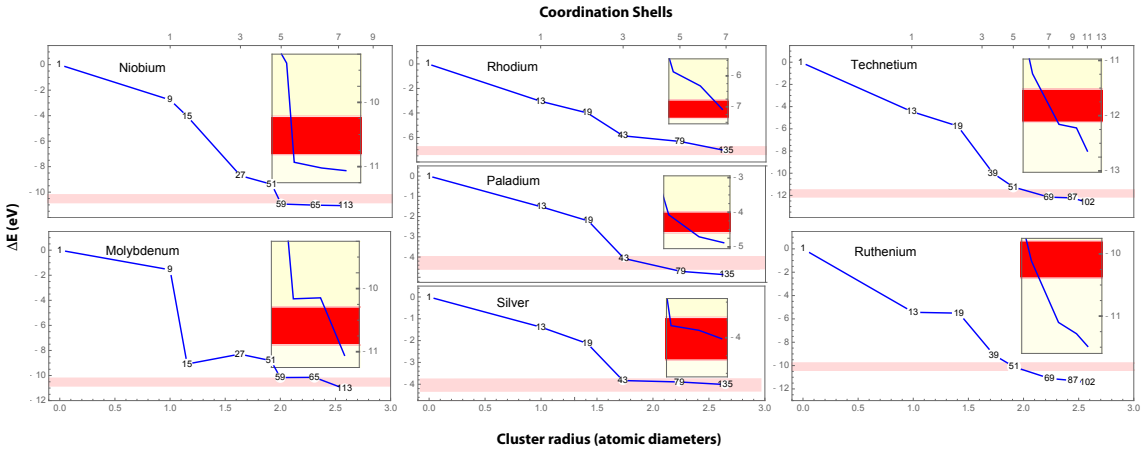

Fig. 5. The change in central Bader atom energy resulting from additional cluster coordination shells (ΔE) for the BCC (left column), FCC (center column) and HCP (right column) 4*d* transition metals. The red stripes indicate a range for the crystalline formation energy of ± 0.3 eV arising from different basis sets. Insets provide a higher fidelity depiction of ΔE for the three largest clusters of the series.

Consider as a first case the similarities in the form of ΔE for the BCC metals Nb and Mo. Recall that the central nine atom cluster of a BCC metal closes at 59 atoms or equivalently five coordination spheres and 2.0 atomic diameters. Figure 5 reveals a rapid decrease of more than an eV in the central cluster energy on addition of the fifth coordination sphere—transforming a 51 to a 59 atom cluster; and for both Nb and Mo bringing the central cluster energy to within 0.3 eV of the estimated formation energy. While in V (Fig. 3) the effect is not as dramatic, a similar central cluster stabilization is observed. This substantive change in ΔE is indicative of a strong coupling between the central nine atom cluster and the region extending from the fifth coordination sphere.

In addition to these similarities there are notable differences, most striking is the stabilization of the central cluster Ω by the third and fourth coordination shells. For Mo there is a dramatic stabilization of Ω with the addition of the third coordination shell, while for Nb and V the same stabilization results from the addition of the third and fourth coordination shells. These variations reflect stronger coupling between Ω and its immediate surroundings in Mo compared to Nb and V. A relevant consequence for such a variation is that in Mo the effects of a perturbation altering the positions of a few atoms will be more localized than those from the same perturbation in Nb or V.

The decay of $\Delta\varepsilon$ for the FCC metals—shown in the center column of Fig. 5—also exhibit similar forms. Notably, the closing of Ω at five coordination spheres and 79 atoms is well

inside the region of asymptotic decay for all the FCC metals modeled (Al, Cu, Rh, Pd, Ag). And it is at this size that the energy of Ω falls to within 0.15 eV of the estimated formation energy for all the 4*d* FCC transition metals. However, more striking is the central cluster stabilization from the third coordination shell, which for the 4*d* transition metals accounts for the bulk of the stabilization energy. This stabilization can be attributed to the partial closing of Ω.

Unlike the BCC metals, characterized by a single type of local minimum, the FCC metals have two: the first at the center of the FCC octahedral hole, and the second at the center of the FCC tetrahedral hole. The tetrahedral holes of the central atom form with the addition of the first coordination sphere and the central atom octahedral holes with the second coordination sphere. The addition of the third coordination sphere at a cluster size of 43 atoms completes all the tetrahedral holes of Ω. And obviously the octahedral holes of Ω are completed at the same time as the closing of Ω with the addition of the fifth coordination shell. Even so, unlike Cu, for the 4*d* FCC metals, there is little coupling between the central cluster and the fifth coordination shell. Hence, just as in the case of the BCC metals, the energy of a perturbation to a small number of atoms in the FCC transition metals will be differentially distributed in accordance with metal's stabilization function. Particularly relevant to our subsequent discussion, perturbation energy will be more delocalized in Cu compared to the 4*d* FCC metals.

Lastly, turning to the modeled HCP transition metals where there are four symmetry unique local minima adjacent to Ω. Like the FCC structure there are both tetrahedral and octahedral minima. And like the FCC metals, the onset of exponential decay begins with the addition of the second coordination sphere. However, with Ω possessing D_{3h} symmetry, the octahedral and tetrahedral holes are split into symmetry unique pairs depending on their displacement perpendicular or parallel to the 3-fold axis. The central thirteen atom cluster undergoes significant closure with the third coordination shell and completely closes with the fifth coordination shell—a cluster of 51 atoms. And beyond which, the stabilization energy due to successive coordination spheres is a fraction of an eV.

The key point is that across all structure types modeled, the energy of Ω "improves" in lock step with its progressive closing, and changes by a fraction of an eV when the surrounding fully close the cluster at a radius of 2.5 to 3 atomic diameters. In other words, the size of the neighborhoods principally responsible for controlling cohesive properties in all types of crystals, regardless of the element or structure, is the same. The precise form of the stabilization function depends on the arrangement of local charge density minima within this volume.

5. Defect Neighborhoods

Defects play a significant role in dictating the properties and performance of materials. For example, the theoretical strength of mild steel, correlated with its Young's Modulus, ranges anywhere from 10-40 GPa [28]. However, its measured tensile strength is much lower - between 0.7-2.1 GPa. This discrepancy between theoretical strength and measured strength is attributed to structural defects in the material.

Amongst the more important structural defects affecting performance in metals are dislocations and grain boundaries. A grain boundary is the region of transition between two atomic arrangements and may be manipulated to enhance strength. Dislocations are characterized by a partially missing plane of atoms. Their production and mobility, which is the source of plastic deformation, also influence strength. Inhibiting their motion can lead to undesirable properties such as brittle failure. This is sufficient evidence to believe that these defect structures inherently possess functionality, and to determine defect neighborhoods wherein such energy dependent properties can be localized, we now turn to investigating the central

cluster energy evolution in these systems.

5.1. Al Edge Dislocation.

An Al edge dislocation was generated via molecular dynamics (see SI). Ω for this structure was defined to be the 9-atom cluster centered on the non-crystallographic hole intrinsic to the defect. As in the crystalline studies, we computed the per atom stabilization function (ΔE) for this cluster through the addition of successive coordination shells (though a coordination shell is somewhat arbitrarily defined for a non-crystalline system) about the central cluster Ω. The calculated energies and specific structure geometries are summarized in the SI and the results are shown graphically in Fig. 6.

We observe that Ω is closed by the coordination shell that is 57 atoms and about 2.2 atomic diameters distant from the cluster center. At this point, the adjoining cages that have one of the atoms in Ω as a vertex are complete. Beyond this critical cluster size, the central cluster energy increases and then, as in the crystalline case, appears to asymptotically approach E_∞, which denotes the energy of Ω when contained in an extended system.

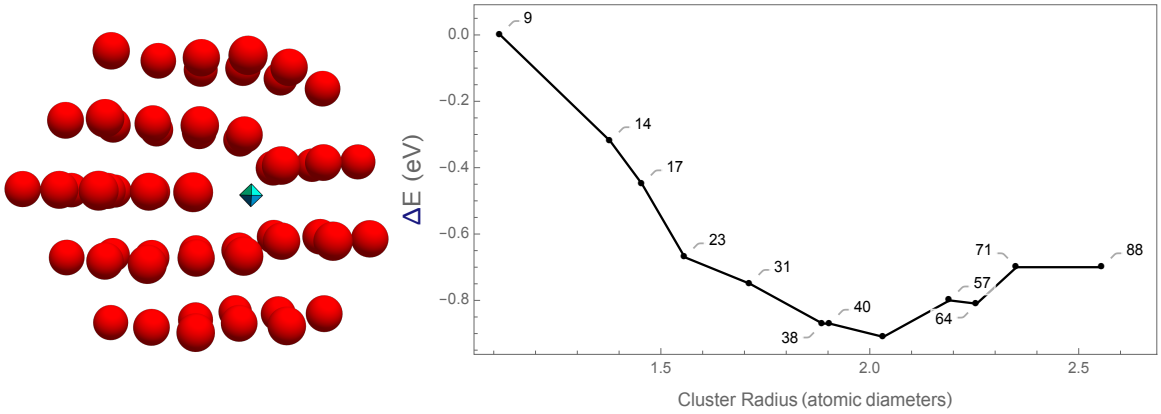

Fig. 6. Schematic representation of Al edge dislocation critical cluster - the red spheres indicate atoms and the cyan octahedron indicates the cage point on which the cluster is centered (left). Change in Bader energy per atom (ΔE) for hole-centered Ω resulting from additional dislocation cluster coordination shells. Callouts indicate number of atoms constituting the representative clusters. (right)

Not unlike the crystalline calculations, the central cluster of the dislocation undergoes stabilization as we grow its surrounding coordination shells. From Fig. 6, it is clear that the central cluster Ω undergoes a stabilizing effect up until it is closed—at which point subsequent addition of atoms destabilize Ω. This is visibly evident from the increase in ΔE beyond 2.0 atomic diameters. As the system as a whole must adopt an electronic distribution of lowest energy, this destabilizing effect is permitted only if there is an offsetting energy lowering of the atoms making up the shells beyond 2.0 atomic diameters.

5.2. Cu and Fe Grain Boundaries.

A well-studied grain boundary both experimentally and computationally is a symmetric 36.8° <001> (310) type tilt boundary in Cu which Duscher *et al.*,[29] determined via atomic resolution x-ray diffraction to be characterized by a repeating kite structure represented schematically in Fig. 7. The atoms immediately adjacent to this site form a roughly pentagonal coordination shell of 14 atoms. We take this 14 atom shell containing a central Cu atom as the central cluster Ω for our investigation. For this symmetric grain boundary coordination, this cluster is dominated by tetrahedral holes arranged in a manner incommensurate with crystal packing [30].

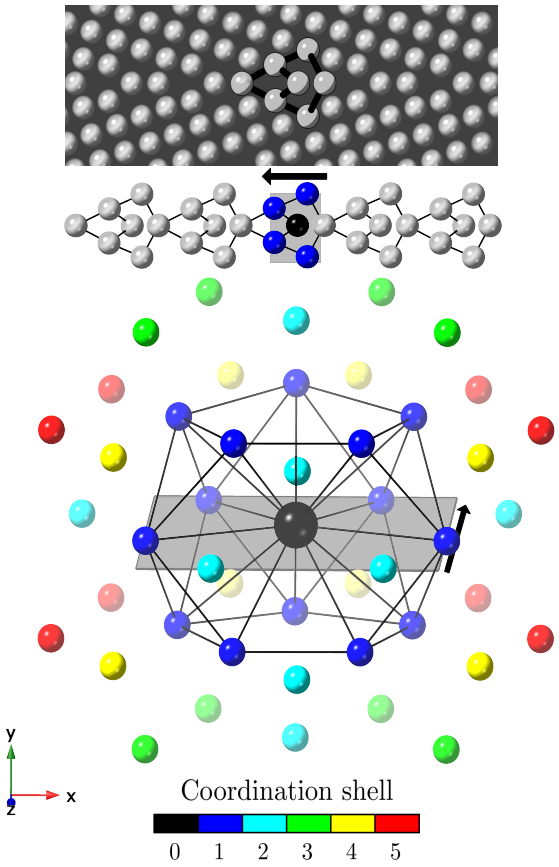

Fig. 7. Depiction of the symmetric 36.8° (310) <001> type tilt boundary cluster. A simulated image of the grain boundary region from reference [29] with the structural unit is indicated (top). The 2-dimensional repeating structural unit (middle), and the corresponding 3-dimensional central cluster with the Cu atom in the center (bottom) are shown. The atoms are color coded based on their positions in the coordination sphere; and the central cluster is represented by the first coordination sphere. The XZ plane, indicated by the gray plane in the bottom frame coincides with the grain boundary plane and corresponds to the grey shaded rectangle in the middle frame, where the same atom coloring is used to show the central cluster atoms in the boundary.

We similarly computed the stabilization function for the central cluster through larger coordinations. The calculated energies are given in the SI and the results are shown graphically in Fig. 8. The grain boundary central cluster is fully closed by the coordination shell 2.3 atomic diameters distant from its center and containing 77 atoms Fig. 9. And as with the crystalline systems, beyond this point the stabilization function for Cu containing clusters appears to be asymptotically converging on E_∞ which we estimate to be at 2.7 atomic diameters and 97 atoms (see SI)[4].

As in the case of the Al dislocation, inspection of Fig. 8 reveals two regions of significant coupling to the Cu containing central cluster. The first region, which again clearly is stabilizing, occurs with the shells between 1.7 atomic diameters containing 23 atoms and 1.9 atomic diameters containing 47 atoms, and correlates to the closing of the non-crystallographically arranged holes adjoining the central cluster (Fig. 9).

[4] using the number of points in Fig. 8, we could more accurately determine E_∞ for the Cu grain boundary than we did for the Al dislocation, thus confirming that ΔE for these defects ultimately converges to E_∞

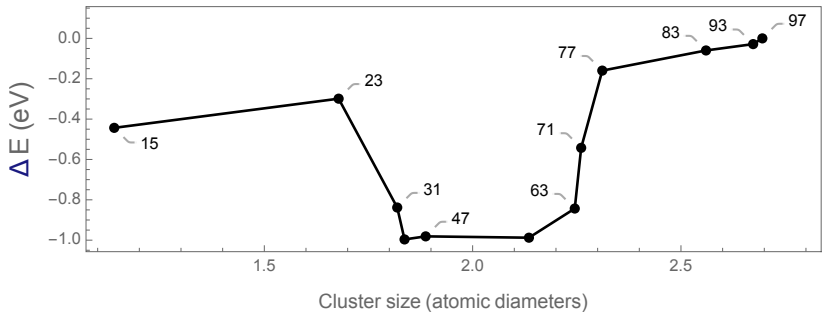

Fig. 8. Change in central cluster Bader energy resulting from additional grain boundary cluster coordination shells. Per atom ΔE for Cu atom centered grain boundary clusters. Callouts indicate number of atoms constituting the representative clusters.

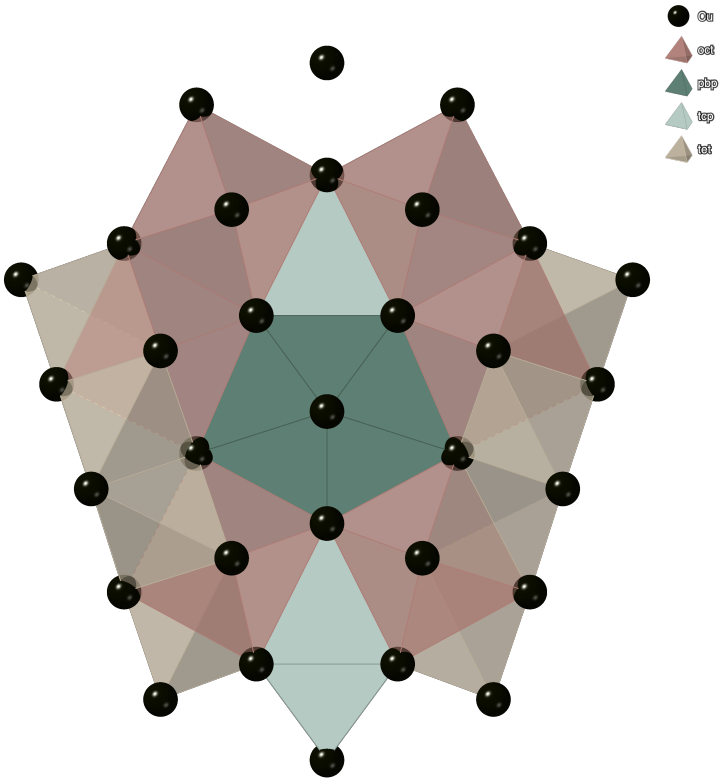

Fig. 9. The polyhedral stacking picture for the 77-atom cluster of FCC symmetric 36.8° <001> (310) type tilt boundary in Cu. The black spheres represent Cu atoms, and the grain boundary is defined by a repeated stacking of hole-centered polyhedra, *i.e.*, trigonal capped prisms (TCP) and pentagonal bipyramids (PBP) [30]. Octahedra (oct) and tetrahedra (tet) from the bulk closest to the grain boundary are now closed at this cluster size.

The second region, which destabilizes the central cluster, occurs with the shells between 2.2 atomic diameters containing 63 atoms and 2.3 atomic diameters containing 77 atoms. Again, this is only possible through an offsetting energy lowering of the atoms making up the shells between 2.2 and 2.3 atomic diameters.

To model another defect neighborhood, we looked at a symmetric 53.1° (210) <001> type tilt boundary in FCC Fe. We chose the central cluster Ω this time encapsulating a grain boundary cage point, defined by a 9-atom trigonal capped prism (Fig. 10). The stabilization function for Ω also reveals a similar trend to the Cu grain boundary calculations. At 1.6 atomic diameters and 29 atoms, the non-crystallographic tetrahedra adjoining the trigonal

capped prism are closed, leading to the characteristic stabilization visible by a decrease in ΔE. Ω in this case is closed at 1.8 atomic diameters and 41 atoms—when the tetrahedral and octahedral cages immediately adjoining Ω are closed.

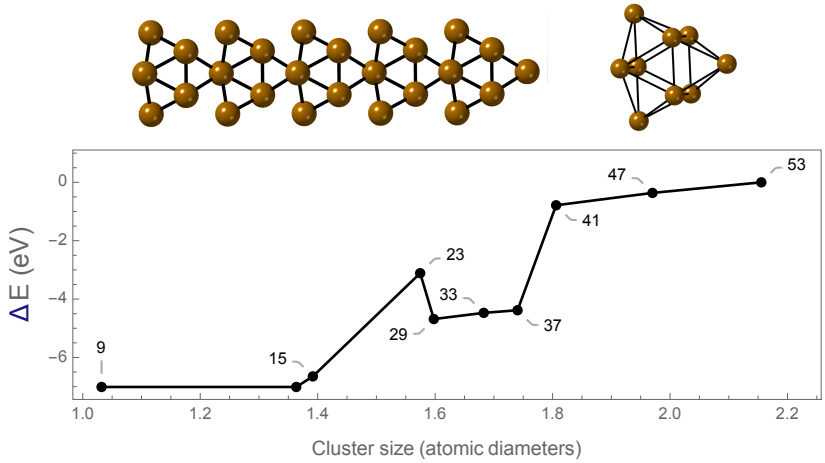

Fig. 10. Schematic representation of the grain boundary and its 9-atom central cluster (top). Change in central cluster Bader energy resulting from additional grain boundary cluster coordination shells for FCC Fe. ΔE for Fe cage-centered grain boundary clusters. Callouts indicate number of atoms constituting the representative clusters.

6. A Functional Group Perspective of Defect Stability

We hypothesize that the local structure of metals is mediated by the surrounding neighborhood extending 2 to 3 atomic diameters distant. In further support of this hypothesis we point to experimental and computational investigations of lattice relaxations [31–33] showing that only the first four or five atomic layers (3 atomic diameters) adjacent to a clean surface show measurable shifts from their bulk spacings. In fact, shifts of the fourth and fifth layer are observed at cryogenic temperatures as they are comparable to the amplitude of room temperature lattice vibrations. Also noteworthy is the experimental and theoretical evidence that the structure of small metallic clusters is far from crystallographic [34–39]. For example, experimental characterization to determine the structure for Ag and Fe microclusters showed that clusters that have radii less than 3 atomic diameters are inconsistent with crystal packing [39].

This hypothesis invites a functional group interpretation of metallic behavior. We have identified two broad metallic functionalities: one crystalline and one defect. Both are contained in neighborhoods roughly 3 atomic diameters in radius. Using the Cu grain boundaries to illustrate, crystalline atoms are essentially blind to grain boundaries more distant than 3 atomic diameters. The same is true of atoms located on the grain boundary, which cannot see the crystalline atoms 3 atomic diameters away. However, the atoms in this three atomic diameter "frontier" region see both environments. These atoms are frustrated by the fact that the alignment of the d-orbitals that maximally stabilize the crystalline functionality differ from the alignment that stabilize the grain boundary environment. Simple group-theoretical arguments will help to clarify this conjecture.

The local symmetry about the center atom of the grain boundary cluster depicted in Fig. 7 is approximately D_{5h}, giving a natural coordinate system, (**X, Y, Z**), in which the **Z**-direction is aligned with the pentagonal axis (a <310> direction) and the **XY**-plane is coincident with the grain boundary plane. As a consequence, the d-orbitals on this central atom will be split into three sets. The first containing the $d_{\mathbf{Z}^2}$ orbital, the second containing $d_{\mathbf{XZ}}$ and

$d_{\mathbf{YZ}}$ orbitals, and the third containing the $d_{\mathbf{XY}}$ and $d_{\mathbf{X^2-Y^2}}$ orbitals. Importantly, linear combinations of the elements of the second set will always produce two nodal planes, one in the grain boundary plane and another in a perpendicular plane containing the **Z**-axis. Linear combinations of the elements of the third set will also produce two perpendicular nodal planes that will intersect along the **Z**-axis.

On the other hand, the natural crystalline coordinate system, (x, y, z), will align with the <001> directions to produce two d-orbital sets: the first containing the d_{xy}, d_{xz}, and d_{yz} orbitals, and the second containing the d_{z^2} and $d_{x^2-y^2}$ orbitals. Each element of the first set has two perpendicular nodal planes drawn from the family of {100} planes, while linear combinations of the second set produce perpendicular nodal planes drawn from the family of {110} planes.

Interactions between atoms are maximized through the alignment of their respective nodal planes [40]. Such orientations optimize orbital overlap and thereby lower the system energy. Hence, enhanced stability for the atoms of the frontier region between the grain boundary and the bulk crystal will be achieved by either aligning nodal surfaces with the grain boundary (**X, Y, Z**) frame or by aligning them with the crystalline (x, y, z) frame. In general, the simultaneous alignment with both frames is geometrically impossible, leading to the frustration apparent in the Cu grain boundary stabilization function of Fig. 8.

Inspection of Fig. 8 reveals that the energy of the central 15 atom cluster is decreased by successive coordination spheres until reaching a cluster size of about 47 atoms. Through this process the atomic d-orbitals of the surrounding coordination spheres align themselves with the (**X, Y, Z**) frame so as to optimize their overlap with the grain boundary atoms. However, the central cluster energy begins to increase for cluster sizes beyond 2.1 atomic diameters—dramatically so for cluster between 63 and 77 atoms. As the central cluster sees the enlarging crystalline environment, speaking anthropomorphically, the atoms of the first coordination shell of the central cluster choose to aligning their d-orbitals with the crystalline (x, y, z) frame and promote crystalline stability at the expense of the local boundary environment. It is noteworthy that at a cluster size of 77 atoms, the crystalline octahedra and tetrahedra closest to the grain boundary are closed (Fig. 9). We have previously shown that these polyhedra and their stacking are important in describing the stability of transition metals [41], and now find that they play a role in mediating defect stability as well.

Note that the stability functions for all the defects modeled show a stabilizing effect from the nearest coordination spheres followed by a destabilizing effect as the crystalline environment grows. Thus, depending on the structure and underlying chemistry of a defect, frontier atoms may either promote local or crystalline stability. The extent of this competition seems to us to be an important factor influencing defect properties and motivated our preliminary investigation of Bi-doped FCC symmetric 36.8° <001> (310) type tilt boundary in Cu.

Bi atoms segregate to and embrittle Cu grain boundaries [42–46]. Shown in Fig. 11 is a comparison of the stabilization function for the pure copper boundary (shown previously as Fig. 8) with one in which the central Cu atom—a known site for Bi segregation [29]—has been replaced with a Bi atom. It is evident that the Bi-doped Cu grain boundary does not possess the region over which the local structure is destabilized, indicating that Bi more strongly aligns the d-orbitals of the Cu atoms in its first coordination shell with the local coordinate frame at the expense of the crystalline structure. Though further work is needed, this stabilization behavior may be a characteristic of embrittling segregants. This result partially supports the argument presented by Eberhart and Vvedensky [47] on the directionality of orbital overlap to predict such embrittlers in grain boundaries, and Haydock's bond mobility model [48] evoking near-neighbor solute-solvent interaction as an indicator of embrittling behavior.

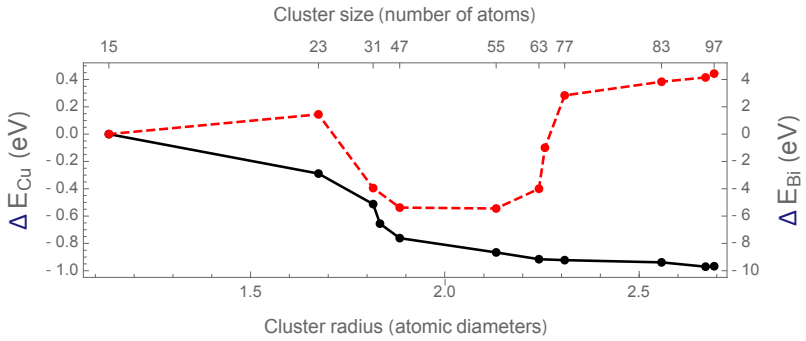

Fig. 11. The central cluster energy evolution for Bi-doped Cu FCC symmetric 36.8° <001> (310) type tilt boundary (black) compared with the undoped calculation in Fig. 8 (red).

7. Conclusions

We have recovered neighborhoods associated with crystals, dislocations, and grain boundaries that we interpret as environmentally insensitive metallic functionalities characterized by well defined energies and energy related properties. From the calculations presented here, it appears that regardless of their local structure, metallic functional groups have a universally similar neighborhood size—asymptotically converging on a defect or crystalline formation energy within a radius of 2 to 3 atomic diameters.

In organic chemistry the concept of functionality forms the conceptual basis from which to understand and predict the properties of large and complex structures such as proteins and enzymes. The advantage in this approach is realized by picturing properties as arising from individual neighborhoods a few atoms in diameter. In contrast, at the electronic level, complex metallic systems containing numerous interacting defects are seen as monolithic units that are computationally cumbersome to analyze. Our work has demonstrated that it may be possible to decompose these complex metallic structures into simpler functional groups that may be studied one at a time, and whose interactions are determined by the few atoms along the boundaries separating these neighborhoods.

We used our non-standard approach to investigate the mechanism through which impurities at a boundary (or other defect) affect behavior. Specifically, we presented preliminary results from electronic structure calculations of a Bi-doped FCC symmetric 36.8° <001> (310) tilt boundary of Cu, which demonstrated that Bi acts to intensify the orbital overlap of the local grain boundary functionality at the expense of the crystalline structure. This may be indicative of embrittling behavior, as Bi is known to embrittle Cu grain boundaries.

Our work has shown the functionality concept is applicable to metals and alloys, and that this methodology can be applied to study a broader range of structures and solute effects, which will be the subject of a future paper. We believe these functional neighborhoods serve as powerful models for further and more chemically based investigations to uncover the relationships between electronic structure and the mechanical response of metallic materials.

Author Contributions

M. Rajivmoorthy: Investigation, formal analysis, visualization, validation, writing – original draft, review & editing; T. R. Wilson: formal analysis, visualization, writing – review & editing; M. E. Eberhart: conceptualization, methodology, supervision, investigation, writing – original draft, review & editing.

Acknowledgments

The authors would like to acknowledge the contribution of Dr. Garritt Tucker and Jacob Tavenner from the Computational Materials Science and Design group at the Colorado School of Mines for providing grain boundary and dislocation structures. We also acknowledge valuable discussions with Dr. Travis Jones from the Fritz Haber Institute of the Max Planck Society.

Funding

Support of this work under ONR Grant No. N00014-10-1-0838 is gratefully acknowledged.

Data Availability

The raw and processed data required to reproduce these findings are accessible from the supplementary information.

1. H. Ago, T. Kugler, F. Cacialli, W. R. Salaneck, M. S. Shaffer, A. H. Windle and R. H. Friend, *J. Phys. Chem. B*, 1999, **103**, 8116–8121.
2. S. P. Collins, T. D. Daff, S. S. Piotrkowski and T. K. Woo, *Sci. Adv.*, 2016, **2**, e1600954.
3. Y. Arima and H. Iwata, *J. Mater. Chem.*, 2007, **17**, 4079–4087.
4. R. F. Bader and P. Beddall, *J. Chem. Phys.*, 1972, **56**, 3320–3329.
5. R. F. Bader, *Atoms in Molecules: A Quantum Theory*, Clarendon Press: Oxford, UK, 1990.
6. R. F. Bader, *J. Phys. Chem. A*, 2008, **112**, 13717–13728.
7. R. Bader and P. Beddall, *Chem. Phys. Lett.*, 1971, **8**, 29–36.
8. P. G. Mezey, *Mol. Phys.*, 1999, **96**, 169–178.
9. N. Sablon, F. De Proft and P. Geerlings, *J. Phys. Chem. Lett.*, 2010, **1**, 1228–1234.
10. S. Fias, F. Heidar-Zadeh, P. Geerlings and P. W. Ayers, *Proceedings of the National Academy of Sciences*, 2017, **114**, 11633–11638.
11. I. S. Bushmarinov, K. A. Lyssenko and M. Y. Antipin, *Russ. Chem. Rev.*, 2009, **78**, 283–302.
12. C. Gatti, *Phys. Scr.*, 2013, **87**, 048102.
13. *The Quantum Theory of Atoms in Molecules: From Solid State to DNA and Drug Design*, ed. C. F. Matta and R. J. Boyd, Wiley-VCH Verlag GmbH & Co. KGaA: Weinheim, 2007.
14. E. Prodan and W. Kohn, *Proc. Natl. Acad. Sci. U.S.A.*, 2005, **102**, 11635–11638.
15. E. Prodan, *Phys. Rev. B*, 2006, **73**, 085108.
16. A. N. Alexandrova, *Chem. Mater.*, 2017, **29**, 8555–8565.
17. W. Kohn, *Phys. Rev. Lett.*, 1996, **76**, 3168–3171.
18. Y. Wang, G. M. Stocks, W. A. Shelton, D. M. C. Nicholson, Z. Szotek and W. M. Temmerman, *Phys. Rev. Lett.*, 1995, **75**, 2867–2870.
19. A. Thiess, R. Zeller, M. Bolten, P. H. Dederichs and S. Blügel, *Phys. Rev. B*, 2012, **85**, 235103.
20. L. Pauling, *The Nature of the chemical bond and the structure of molecules and crystals : an introduction to modern structural Chemistry*, Cornell University Press, 1939.
21. A. D. McNaught, A. Wilkinson *et al.*, *Compendium of chemical terminology*, Blackwell Science Oxford, 1997, vol. 1669.
22. J. I. Rodríguez, P. W. Ayers, A. W. Götz and F. L. Castillo-Alvarado, *J. Chem. Phys.*, 2009, **131**, 021101.
23. G. te Velde, F. M. Bickelhaupt, E. J. Baerends, C. Fonseca Guerra, S. J. A. van Gisbergen, J. G. Snijders and T. Ziegler, *J. Comput. Chem.*, 2001, **22**, 931–967.
24. E. J. Baerends, T. Ziegler, A. J. Atkins, J. Autschbach, D. Bashford, A. Bérces, F. M. Bickelhaupt, C. Bo, P. M. Boerrigter, L. Cavallo, D. P. Chong, D. V. Chulhai, L. Deng, R. M. Dickson, J. M. Dieterich, D. E. Ellis, M. van Faassen, L. Fan, T. H. Fischer, C. F. Guerra, M. Franchini, A. Ghysels, A. Giammona, S. J. A. van Gisbergen, A. W. Götz, J. A. Groeneveld, O. V. Gritsenko, M. Grüning, S. Gusarov, F. E. Harris, P. van den Hoek, C. R. Jacob, H. Jacobsen, L. Jensen, J. W. Kaminski, G. van Kessel, F. Kootstra, A. Kovalenko, M. V. Krykunov, E. van Lenthe, D. A. McCormack, A. Michalak, M. Mitoraj, S. M. Morton, J. Neugebauer, V. P. Nicu, L. Noodleman, V. P. Osinga, S. Patchkovskii, M. Pavanello, C. A. Peeples, P. H. T. Philipsen, D. Post, C. C. Pye, W. Ravenek, J. I. Rodríguez, P. Ros, R. Rüger, P. R. T. Schipper, H. van Schoot, G. Schreckenbach, J. S. Seldenthuis, M. Seth, J. G. Snijders, M. Solà, M. Swart, D. Swerhone, G. te Velde, P. Vernooijs, L. Versluis, L. Visscher, O. Visser, F. Wang, T. A. Wesolowski, E. M. van Wezenbeek, G. Wiesenekker, S. K. Wolff, T. K. Woo and A. L. Yakovlev, *ADF2016, SCM, Theoretical Chemistry, Vrije Universiteit, Amsterdam, The Netherlands*, 2016.
25. G. te Velde and E.J. Baerends, *Phys. Rev. B*, 1991, **44**, 7888.
26. G. Wiesenekker and E.J. Baerends, *J. Phys. Condens. Matter*, 1991, **3**, 6721.
27. M. E. Eberhart, *Struct. Chem.*, 2017, **28**, 1409–1417.
28. G. E. Dieter and D. J. Bacon, *Mechanical metallurgy*, McGraw-hill New York, 1976, vol. 3.
29. G. Duscher, M. F. Chisholm, U. Alber and M. Ruhle, *Nat. Mater.*, 2004, **3**, 621–626.
30. M. Ashby, F. Spaepen and S. Williams, *Acta Metall.*, 1978, **26**, 1647–1663.
31. T. Ning, Q. Yu and Y. Ye, *Surf. Sci.*, 1988, **206**, L857–L863.
32. J. Wan, Y. Fan, D. Gong, S. Shen and X. Fan, *Model. Simul. Mater. Sci. Eng.*, 1999, **7**, 189.
33. R. P. Gupta, *Phys. Rev. B*, 1981, **23**, 6265.
34. F. Baletto, *J. Phys. Condens. Matter*, 2019, **31**, 113001.
35. M. L. Cohen, M. Chou, W. Knight and W. A. De Heer, *J. Phys. Chem.*, 1987, **91**, 3141–3149.
36. K. Clemenger, *Phys. Rev. B*, 1991, **44**, 12991.
37. W. A. de Heer, W. Knight, M. Chou and M. L. Cohen, *Solid State Phys.*, 1987, **40**, 93–181.
38. P. Montano, J. Zhao, M. Ramanathan, G. Shenoy and W. Schulze, *Small Particles and Inorganic Clusters*, Springer, 1989, pp. 103–105.
39. G. Wertheim, *Small Particles and Inorganic Clusters*, Springer, 1989, pp. 319–326.
40. R. Hoffmann and R. B. Woodward, *Acc. Chem. Res.*, 1968, **1**, 17–22.
41. S. K. Riddle, T. R. Wilson, M. Rajivmoorthy and M. E. Eberhart, *Molecules*, 2021, **26**, 5396.
42. A. Hallowes and E. Voce, *J. Inst. Met.*, 1947, **73**, 323–376.
43. A. Donald and L. Brown, *Acta Metall.*, 1979, **27**, 59–66.
44. J. Russell and A. Winter, *Scripta Metall.*, 1985, **19**, 575–579.
45. U. Alber, H. Müllejans and M. Rühle, *Acta Mater.*, 1999, **47**, 4047–4060.
46. W. Sigle, L.-S. Ciiang and W. Gusr, *Philos. Mag., A*, 2002, **82**, 1595–1608.
47. M. Eberhart and D. Vvedensky, Materials Science Forum, 1989, pp. 169–186.
48. R. Haydock, *J. Phys. C: Solid State Phys.*, 1981, **14**, 3807.